Structure and bonding in crystalline and molten Li-Sn alloys: A first-principles density-functional study

O. Genser and J. Hafner
Institut für Materialphysik and Center for Computational Materials Science, Universität Wien, Sensengasse 8/12, A-1090 Wien, Austria
(Received 4 October 2000; published 23 March 2001)

Ab-initio local-density-functional investigations of crystalline and molten Li-Sn alloys at equiatomic compositions and a stoichiometry close to Li_4Sn (allowing to complete the octet-shell of the Sn-ions if complete charge-transfer is assumed) have been performed. The aim of these studies is to investigate the influence of the formation of direct covalent Sn-Sn bonds on the structure and stability of the alloys. At the equiatomic composition we find that the monoclinic LiSn structure with the Sn-atoms forming rumpled layers (like those in crystalline As) is more stable than a simple ionic CsCl lattice; in the molten phase, this is reflected by the formation of a dense disordered network of Sn-Sn bonds. At the octet composition, an ionic structure with no direct Sn-Sn neighbors and a partially covalent structure with Sn_2 dimers are of comparable stability. In the molten phase, the importance of covalent Sn-Sn bonding is reduced and only a small fraction of the dimers present in the crystal structure survive. Detailed *ab-initio* molecular dynamics studies for the structural, dynamic, and electronic properties of the liquid alloys are presented. The results are discussed in relation to a generalized Zintl principle for structure and bonding in such strongly interacting alloy systems.

DOI: 10.1103/PhysRevB.63.144204 PACS number(s): 61.25.Mv, 71.15.Pd, 61.66.−f, 71.20.Gj

I. INTRODUCTION

The alloys of the alkali metals with the post-transition-group IV elements display rather complex phase diagrams and very peculiar variations of the chemical bonding and of the structural, thermodynamic and electronic properties as a function of composition. Alloys of the heavier alkalis (K, Rb, Cs) with all group-IV elements exhibit clustering of the group-IV atoms into polyanions (Zintl-ions). The formation of polyanions is usually explained in terms of the Zintl principle:[1,2] The alkali atoms donate their single valence electron to the more electronegative group-IV atoms which become isoelectronic to the P atom and form tetrahedral clusters, in analogy with the P_4 molecule. The Fermi-level falls into a narrow gap separating bonding and antibonding electronic states of the tetrahedra, explaining the electronic anomalies observed at the equiatomic compositions. The role of the alkali ions is to keep the polyanions apart and to prevent inter-tetrahedral interactions which would tend to close the gap. Detailed electronic structure calculations for alloys of the alkali metals with Pb[3,4], Sn[5], and Ge and Si[6] have confirmed the validity of the Zintl principle for the equiatomic compounds and demonstrated that only for the alloys of K, Rb, and Cs the size of the alkali atoms is sufficient to stabilize the polyanionic phase over structures that are much closer to a simple ionic picture of positive alkali and negative group-IV ions. Experimental work[7–9] suggested that at least a fraction of the polyanionic clusters survives at temperatures not too far above the melting point. For NaSn and CsPb, it was shown that melting occurs via the formation of an intermediate ''plastic phase'' in which the alkali atoms are supposed to diffuse freely, while the group-IV polyanions perform only rotational or librational movements.[10] Verification of the conjecture of the existence of polyanions in the disordered phases by *ab-initio* molecular dynamics simulations on molten KSi[11] and NaSn[12–14] turned out to be extremely difficult, the results suggested the existence of a disordered network of the electronegative group-IV atoms rather than the existence of well defined polyanions. Only very recently ab-initio simulations on equiatomic (K, Na, Li)-Sn alloys brought evidence for a survival of polyanions in KSn, to a much lesser degree in NaSn, but not in LiSn.[15,5] However, in both NaSn and LiSn, strong interactions between the Sn atoms lead to the formation of a covalently bonded network in the liquid phase.

The chemical bonding in Li-group-IV alloys turns out to be different from that in the alloys of the heavier alkali metals. In the phase diagram of Li-Pb alloys[16] the most stable intermetallic compounds are found around the ''octet'' composition Li_4Pb, at which a formally complete electron transfer would allow to complete the rare-gas shell of the Pb^{4-} anion. The crystal structures of these ''near-octet'' compounds ($Li_{22}Pb_5$, Li_7Pb_2, Li_3Pb, Li_8Pb_3) are characterized by a purely heteroionic coordination of the Pb atoms by Li only. The same salt-like bonding principle also applies to the equiatomic LiPb compound which exhibits a CsCl structure. The phase diagram of Li-Sn alloys[17] exhibits stable compounds at essentially the same compositions, but neither the octet nor the equiatomic compounds are isostructural to the Li-Pb alloys: the congruently melting near-octet compounds have both 7:2 stoichiometry, but Li_7Pb_2 crystallizes in a hexagonal structure (Pearson symbol hP9)[18] with no Pb-Pb nearest neighbors, whereas Li_7Sn_2 adopts a more complex orthorhombic structure (Pearson symbol oC36)[19] with part of the Sn atoms forming Sn_2 dimers. According to Zalkin and Ramsay,[18] the structure of Li_7Pb_2 may be considered as being derived from the structure of pure Li, with a fraction of the Li atoms being substituted by Pb and with small displacements from the ideal lattice positions. The important point is that in the hexagonal Li_7Pb_2 structure there are no direct Pb-Pb neighbors. Frank *et al.*[19] have pointed out that the rows of Li and group-IV atoms found in the basal plane of hexagonal Li_7Pb_2 exist also in orthorhombic Li_7Sn_2, but

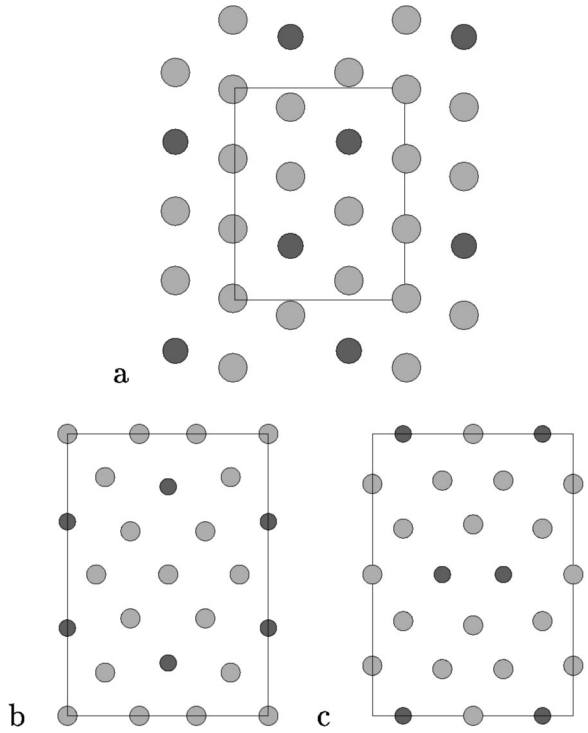

FIG. 1. Structural relationship between the Li_7Sn_2 (oC36) and Li_7Pb_2 (hP9) structures. (a) shows the atomic arrangement in a plane of the hexagonal Li_7Pb_2 structure spanned by the [001] and $[\bar{1}10]$ axes. (b) and (c) show the atoms in planes perpendicular to the *c*-axis located at $z=0$ and $z=0.5$. Empty circles represent Li-atoms, shaded circles Sn-atoms. The characteristic feature are the vertical rows of atoms: every third atomic row contains only Li atoms, while in the other rows every third atom is a Sn-atom. The two structures differ by the relative displacement of the atomic rows with respect to each other, cf. text.

they are displaced with respect to each other in such a way that half of the Sn atoms form Sn_2 pairs (see Fig. 1 and below). A similar structural relationship exists also between the CsCl-structure of LiPb and the LiSn-structure,[21,20] but due to their higher concentration, the Sn-atoms now form corrugated atomic planes similar to those found in the As-structure. The formation of such structures may be interpreted in terms of a generalized Zintl principle.[1,22–24] At the exact octet composition, complete electron transfer would lead to the formation of Sn^{4-} anions with a rare-gas configuration and a salt-like structure. At the stoichiometry 7:2, only half of the Sn-atoms can complete their octet shell, the remaining Sn-atoms becoming isoelectronic to halogen atoms. The formation of Sn_2^{2-} dimers corresponds to the formation of diatomic molecules in the halogen crystals. In the equiatomic compounds, electron transfer leads to the formation of Sn^--ions isoelectronic to pnictide atoms, but due to the higher density As-like corrugated layers and not P_4-like polyanions, are formed. The electronic mechanisms leading to the formation of a sequence of different Zintl compounds within the same alloy system have been discussed by Jank and Hafner[24] at the example of Li-Ga alloys and by Seifert-Lorenz and Hafner[25] for the K-Sb system.

The tendency to form covalent bonds between the group-IV atoms is continued in the alloys of Li with Ge and Si. This is particularly striking in phases such as $Li_{12}Si_7$ where Si_4 and Si_5 polyanions forming stars and pentagons are found.[26] First principles simulations performed for this alloy[27] have shown that in the molten phases a covalently bonded network of Si atoms is formed.

Hence the Li-Sn system presents the opportunity to study the structural and physical properties of an alloy system at the borderline between polyanionic and simple ionic ordering. Molten Li-Sn alloys have been studied using x-ray[28] and neutron diffraction.[29] A distinct prepeak indicating strong chemical ordering has been observed over a wide range of composition. In addition several physical properties including the EMF,[30] the vapor pressure,[31] the electrical resistivity[32] and the Knight shift,[33] have been measured. The excess volume, the electrical resistivity and its temperature derivative, and the Knight shift, show sharp extrema in the octet-composition, and this has been interpreted as indicating ''compound-formation'' in the liquid phase.[29] In the present paper we use *ab-initio* local-density-functional (LDF) techniques to investigate the structural, dynamic, and electronic properties of Li-Sn alloys at the octet and equiatomic compositions, both in the crystalline and liquid phases. Our paper is organized as follows. In Sec. II we give a very brief summary of the methodology and we summarize important technical details. In Sec. III we present the results for crystalline Li_7Sn_2 and LiSn in two different crystal structures with and without direct Sn-Sn neighbors. Sections IV–VI summarize the results of the *ab-initio* molecular dynamics simulations for the structural, dynamic, and electronic properties of the liquid alloys. We summarize in Sec. VII.

II. METHODOLOGY

Our investigations have been performed using the Vienna *ab-initio* simulation package VASP,[34–36] which is based on the following principles: (1) Electronic exchange and correlation are treated in the local-density-approximation (LDA), using the functional developed by Ceperley and Alder as parameterized by Perdew and Zunger.[37] No gradient-corrections have been used because the generalized gradient corrections improve agreement with experiment for the alkali metals, but substantially overshoot for tin. (2) The solution of the generalized Kohn-Sham equations is performed using an efficient iterative matrix-diagonalization routine based on a sequential band-by-band residual minimization method (RMM)[35,38] applied to the one-electron energies. An improved Pulay-mixing[39] was used to achieve self-consistency of charge-density and potential.[35] (3) The optimization of the crystal structure is performed via a conjugate-gradient minimization of the total energy with respect to volume and shape of the unit cell and the internal atomic coordinates, using the analytic Hellmann-Feynman forces acting on the atoms. The structural optimization was stopped when the change in the total (free) energy between two successive steps became smaller than 10^{-3} eV/atom. (4) Ab-initio molecular-dynamics (MD) simulations have been performed for a constant-volume ensemble of 124 particles in a cubic box using a Nosé-thermostat.[40] The equilibrium volume of

the liquid alloys has been derived from a series of short constant-volume simulations at different densities during which the internal pressure was monitored. Extended MD simulations were performed at the zero-pressure density derived from these exploratory runs, carefully monitoring the pressure fluctuations. Integration of the equations of motion in the extended phase-space of Nosé-dynamics was performed using a Verlet algorithm with a time-step of $\Delta t = 3$ fs. MD runs have been started with the atoms distributed over the sites of a simple cubic lattice, using a 5^3 atom supercell with a central vacancy. To accelerate melting, the MD simulation was started at a high temperature of $T = 1500$ K and equilibrated for 1000 time steps ($\equiv 3$ ps). After this initial phase, the temperature was lowered to a value close to the melting point of the crystalline compound and continued at least for 12 ps. (5) The calculations have been performed using fully nonlocal optimized ultrasoft pseudopotentials.[41,42] Details of the pseudopotentials are described in our previous work.[15] In addition, *ab-initio* molecular dynamics simulations have been performed for both liquid metals (Li: Kresse;[43] Sn: Genser and Hafner[44]). The results for the structural, dynamic, and electronic properties are in excellent agreement with experiment. (6) Brillouin-zone integrations were performed using a grid of Monkhorst-Pack special points[45] and the linear tetrahedron method with Blöchl corrections[46] for the crystalline alloys, checking carefully convergence with respect to the number of *k*-points. In the simulations for the liquid alloys, only the Γ-point has been used during the MD-simulations, but the final electronic density of states has been recalculated on a finer *k*-point mesh for a series of representative configurations. (6) The energies calculated as a function of volume were interpolated using a Murnaghan equation-of-state to determine the bulk modulus.[47]

TABLE I. Lattice constants (a, b, c), internal atomic positions and structural parameters; atomic volume Ω; cohesive energy E; volume $\Delta\Omega$ and heat ΔH of formation; bulk modulus B and parameters determining the atomic positions within the unit cell as calculated for Li_7Sn_2 in the experimental orthorhombic structure (Pearson symbol oC36, space group Cmmm), and in the hypothetical hexagonal Li_7Pb_2 (Pearson symbol hP9, space group P321) compared with experiment (numbers in parentheses).

	Li_7Sn_2	Li_7Pb_2
a(Å)	9.590 (9.80)	4.535
b(Å)	13.391 (13.80)	
c(Å)	4.555 (4.75)	8.155
b/a	1.396 (1.408)	
c/a	0.475 (0.484)	1.798 (1.808) [a]
Ω(Å ^{3})	16.3 (17.8)	16.1
$\Delta\Omega$ (%)	−26.5 (−27.0)	−27.8
E (eV/atom)	−3.030	−3.035
ΔH (eV/atom)	−0.444	−0.449
B (kbar)	322	325
Li1	(2a)	(1a)
Li2	(2c)	(2c) $z = 0.325$ (0.333) [a]
Li3	(4g) $x = 0.349$ (0.359)	(2d) $z = 0.422$ (0.417) [a]
Li4	(4j) $y = 0.173$ (0.179)	(2d) $z = 0.102$ (0.083) [a]
Li5	(8p) $x = 0.187$ (0.187) $y = 0.155$ (0.154)	
Li6	(8q) $x = 0.342$ (0.349) $y = 0.162$ (0.165)	
Sn1	(4h) $x = 0.167$ (0.153)	(2d) $z = 0.235$ (0.250) [a]
Sn2 (4i)	$y = 0.317$ (0.313)	

[a]The experimental values for the internal parameters and the axial ratio refer to the Li_7Pb_2 phase.

III. CRYSTALLINE INTERMETALLIC COMPOUNDS

In the following, we present our results for the optimized electronic structure of the near-octet compound Li_7Sn_2 in its stable crystal structure and assuming a Li_7Pb_2 structure, and of the equiatomic compound LiSn in its monoclinic structure and assuming a CsCl lattice.

A. Near-octet compounds

1. Structure and phase stability

A complete optimization of the compound Li_7Sn_2 in its stable crystal structure, and in the Li_7Pb_2 structure, has been performed. Figure 1 summarizes the structural relationship between the two competing phases. In the Li_7Pb_2-structure we find atomic rows parallel to the hexagonal axis. Every third row contains only Li-atoms while the other rows contain both Pb(Sn) atoms, with every third atom in each row being a Pb(Sn) atom. The positions of neighboring rows is such that the distance between the tetravalent atoms is maximized [see Fig. 1(a)]. Similar rows of atoms, which are oriented along the [110] direction exist in the Li_7Sn_2-structure. Within the $z = 0$ plane, the atomic arrangement is similar to that in the base plane of Li_7Pb_2, but in the $z = 0.5$ plane, the polyvalent atoms in adjacent rows form dimers. Blocks of three atomic rows are shifted with respect to each other by one interatomic distance, such that the distance of the isolated Sn atoms in the $z = 0$ plane from the Sn-dimers in the plane above and below is maximized. This results in a tripled periodicity along the [210] direction (corresponding to the $[\bar{1}10]$ direction in the Li_7Pb_2 structure).

The total energies of both phases have been calculated as a function of volume. The results are summarized in Table I and in Fig. 2. The Li_7Pb_2 structure was found to be lower in energy than the Li_7Sn2 lattice, in disagreement with experiment. However, the structural energy difference is only about 5 meV/atom, and shows only a small variation with density. The analysis of the individual contributions to the total energy shows that the Li_7Pb_2 structure leads to a lower Madelung energy, whereas the band-structure contributions favor the Li_7Sn_2 structure. However, the gain in covalent bond energy through the formation of the Sn_2 dimers cannot overcompensate the deficit in the electrostatic energy.

We find that the optimized Li_7Sn_2 structure agrees quite well with the result of the x-ray determination of the stable crystal structure: the most important difference compared to experiment is the underestimation of the lattice parameters

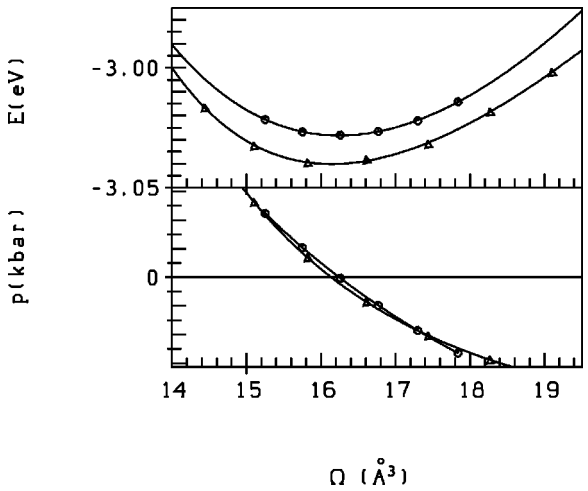

FIG. 2. Energy vs volume for the compound Li_7Sn_2 in its stable oC36 structure (circles) and in a hypothetical Li_7Pb_2 (hP9) structure (triangles). Symbols show the calculated total energies, the full lines a Murnaghan-fit. Cf. text.

by about 2 to 4 pct., which is characteristic for the tendency of the local density approximation for overbinding. On the other hand, the large negative excess volume (calculated with respect to bcc Li and α-tin in the diamond structure, relative to β-tin the volume reduction on alloying would be only 21.7 pct.) is predicted with good accuracy. Optimized internal structural parameters, on the other hand, agree well with experiment. For many materials, generalized gradient corrections (GGC) lead to better results for the lattice parameters; but we have to remember that while for the light elements the GGC's lead to a substantial improvement, they tend to overcorrect for the heavier elements (for results on the alkali metals and Sn we refer to our previous work[5]). Also, it is now well documented[48,49] that the addition of GGC's to the local-density functional lead to an almost isotropic expansion of the equilibrium volume, while at fixed volume the structures calculated in the LDA and LDA +GGC are essentially identical. For this reason, as in our previous work on KSn and NaSn, only the LDA was used in the present work. This difficulty is also reflected in the comparison of the optimized and measured interatomic distances: calculated Li-Li nearest neighbor distances range between 2.59 and 3.59 Å; experimental distances between 2.71 and 3.67 Å. The bond lengths in Li-Sn pairs extend from 2.74 to 3.35 Å (theory) and from 2.81 to 3.51 Å (experiment[19]), respectively. The length of the Sn_2 dimers that exist in this structure is 3.20 Å (theory) compared to 3.00 Å (experiment). It is remarkable that the bond length in the Sn_2 dimers is overestimated in our calculation which produces a too high overall density. To some regard, this reflects the fact that the exchange-correlation functional underestimates the interatomic distances in Li, but reproduces them quite well for Sn, resulting in small but non-negligible distortions of the structure. However, the fact that the calculated bond-length in the Sn_2 dimers is even larger than measured means that the strength of the covalent bond in the Sn-Sn pairs appears to be slightly underestimated.

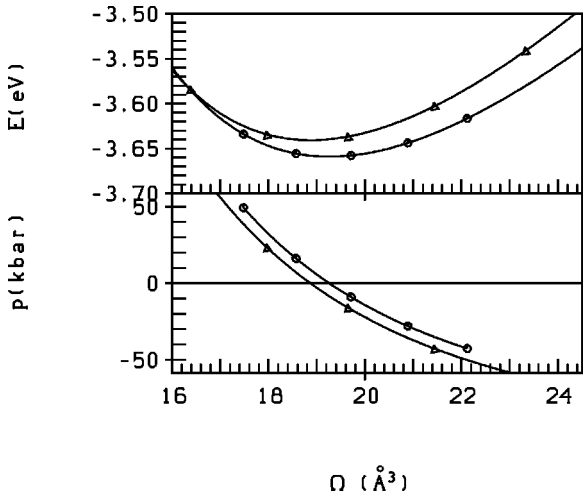

FIG. 3. Energy vs volume for the compound LiSn in its stable mP6 structure (circles) and in a hypothetical CsCl structure (triangles). Symbols show the calculated total energies, the full lines a Murnaghan-fit. cf. text.

2. Electronic spectrum

The total, local, and partial electronic densities of states (DOS) of both competing phases are compared in Fig. 4. A few things should be emphasized. (i) Although the local DOS projected onto atomic spheres surrounding the Li sites is by no means very small (an integration over atomic spheres even shows that charge neutrality is rather well conserved on a local level), it is still legitimate to speak of a charge-transfer compound, in the sense that the valence bands are dominated solely by the strong attractive potential of the Sn-atoms. (ii) At the Sn-sites, the character of the low-lying band centered around -7 eV is Sn-s, that of the band close to the Fermi level Sn-p. At the Li-sites, both bands have strongly mixed s,p,d-character, indicating that the local DOS stems from extended states centered at the Sn-atoms and extending into the Li-spheres. Under these circumstances an attempt to quantify the electron transfer would not make sense. (iii) The characteristic differences between the DOS's of the competing phases is the splitting of the Sn-s band and the larger bandwidth of the Sn-p band for the Li_7Sn_2 phase, resulting from the bonding-antibonding splitting of the states localized on the Sn_2 dimers. This leads to a gain in covalent bond energy. (iv) In both phases, the Fermi level falls very close to a pseudo-gap separating the fully occupied Sn-states from the essentially empty Li-states; the DOS at the Fermi level being lower in the stable phase containing dimers. (v) The bonding-antibonding splitting is probably somewhat underestimated due to a too large bond-length in the Sn_2 dimers. This brings us back to the arguments formulated above.

B. Equiatomic compounds

The case of the equiatomic LiSn alloys was already briefly discussed in our previous work,[5] where the results at equilibrium density have been presented. Here we extend the investigations to the phase-stability as a function of volume (see Fig. 3). As expected, the LDA error is somewhat smaller

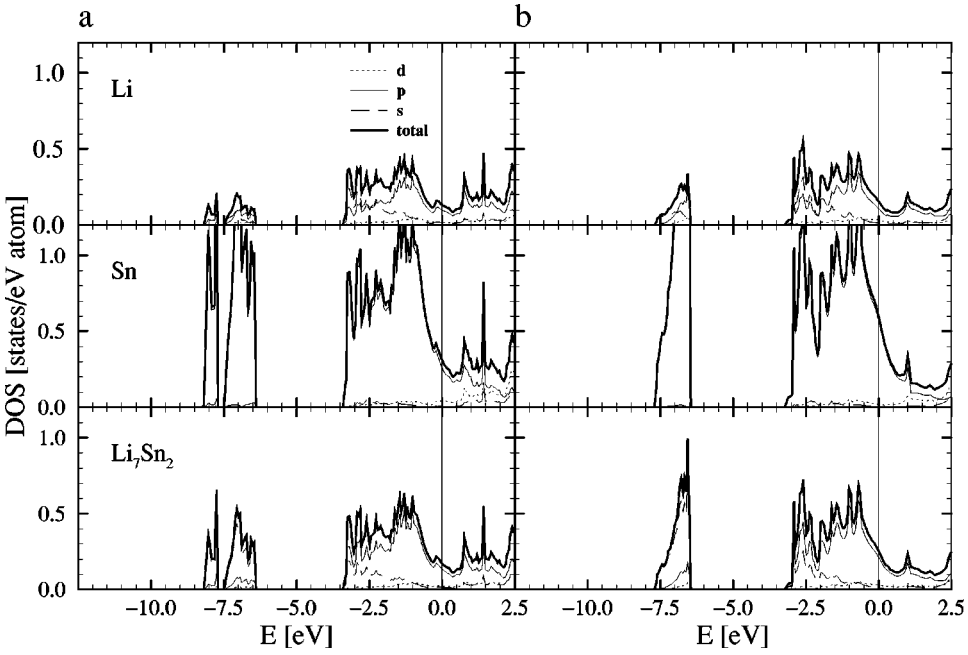

FIG. 4. Total and partial electronic densities of state of Li_7Sn_2 in its stable crystal structure (a) and in the Li_7Pb_2 structure (b), cf. text.

than for the Li-rich near-octet compound, between 0.6 and 3 pct. for the monoclinic lattice constants. Here we compare the LiSn-structure[21] with the CsCl lattice adopted by the compound LiPb. The structural relationship between the two lattices is similar as for the two structures with 7:2 stoichiometry. Both structures are based on identical atomic rows occupied alternatingly by Li and Sn. In the CsCl structure neighboring rows are shifted by 1/2 of the repeat-length such that direct Sn-Sn neighbors are avoided. In the LiSn structure the displacement of neighboring rows is only 1/3 of that distance. This leads to Sn-Sn contacts and the formation of corrugated layers of Sn-atoms intercalated by Li.[21,20]

At zero pressure the monoclinic LiSn-phase is 0.019 eV/atom lower in energy, but under compression the CsCl-phase is increasingly favorized. A pressure-induced phase transition is expected at pressures of about 100 kbar. The higher compressibility of the more compact CsCl-type phase is also reflected by an increased bulk modulus of $B=0.429$ Mbar, compared to $B=0.409$ in the stable LiSn structure. The optimized structural data are summarized in Table II, where we find that the stable structure is well described by the LDA calculations. For all details, we refer to our previous work, where we have also presented a detailed comparison of the electronic structure of both phases. Here we present only a comparison of the total DOS in both structures (see Fig. 5). In analogy to the results for the Li_7Sn_2 and Li_7Pb_2 structures discussed above, we find that the valence states are dominated entirely by Sn-states, but only small differences in the electronic spectra. The Sn-*p* type bands near the Fermi level are virtually identical. The formation of strong covalent Sn-Sn bonds in the stable monoclinic phase merely results in a broadening of both the Sn-*s* band, compared to the purely heteroatomic CsCl-type phase with no direct Sn-Sn bonds. The difference in the electronic spectra of the LiSn- and CsCl-type phases is very pronounced in the equiatomic alloys of the heavier alkalis (where we had found large structural energy differences between the stable polyanionic, the LiSn-type, and the simple ionic CsCl-type phases), but only relatively weak in LiSn where the structural energy difference is only modest.

IV. MOLTEN ALLOYS–ATOMIC STRUCTURE

A. Octet alloys

The first task is the determination of the density at which the constant-volume simulations in the canonical ensemble should be performed. From a series of short MD-runs at different densities we deduce an equilibrium atomic volume

TABLE II. Lattice parameters (a,b,c, β), internal structural parameters,[a] atomic volume Ω, volume and heat of formation $\Delta\Omega$ and ΔH, and bulk modulus B in LiSn-type (Pearson symbol mP6) and CsCl-type LiSn compounds. Experimental values are given in parentheses.

	LiSn-type	CsCl-type
a (Å)	5.041 (5.17)	3.355
b (Å)	3.160 (3.18)	3.355
c (Å)	7.505 (7.74)	3.355
b/a	0.627 (0.615)	1
c/a	1.489 (1.497)	1
β (°)	104.8 (104.5)	90
Ω(Å^3)	19.26 (20.53)	18.87
$\Delta\Omega$ (%)	−26.7 (−26.4)	−28.2
ΔH (eV/atom)	−0.399	−0.381
B (kbar)	409	429
Li1 (2n)	x=0.270 (0.263)	-
	z=0.328 (0.336)	-
Sn2 (2m)	x=0.240 (0.234)	-
	z=0.662 (0.660)	-

[a]The experimental values for the internal parameters and the axial ratio refer to the Li_7Pb_2 phase.

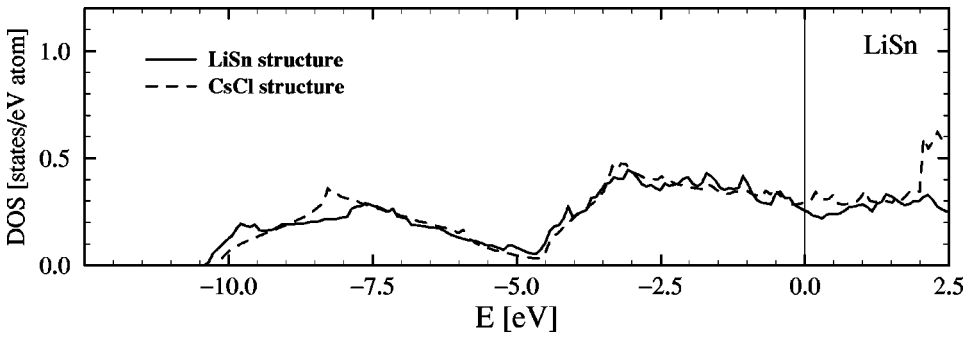

FIG. 5. Total electronic densities of state of LiSn in its stable crystal structure (full line) and in the CsCl structure (dashed line), cf. text.

of $\Omega = 20.68$ Å^3 at $T = 1040$ K, which is considerably smaller than the experimental atomic volumes of both Li ($\Omega = 26.00$ Å^3) and Sn ($\Omega = 29.8$ Å^3) at this temperature. No experimental densities for the liquid alloys are available, but for the crystalline alloys, strong negative excess volumes are calculated (cf. the preceding section). For Li-Pb alloys, where densities have been measured for both crystalline and molten alloys,[50] it has been shown that the excess volumes are comparable. Using the excess volume of Li_7Sn_2 calculated with respect to white tin ($\Delta\Omega = 21.7$ pct.) and the experimental volumes of molten Li and Sn taken from Waseda,[51] we estimate an equilibrium volume of 21.04 Å^3 which agrees reasonably well with the *ab-initio* simulations.

1. Pair correlation functions

Figure 6 presents the results for the partial pair correlation functions of liquid Li_4Sn at $T = 1040$ K and a number density of $n = 0.048$ Å^{-3}, where the vertical bars show the nearest-neighbor distances in the crystalline compound Li_7Sn_2 for comparison. The most striking features are the almost complete absence of a nearest-neighbor peak in the Sn-Sn correlation function; the dominant nearest-neighbor peak for Li-Sn heterocoordination; and the weak, rather broad maximum in the Li-Li correlation functions. All these features agree with a strong, salt-like chemical short-range order. The positions of the first peaks agree rather well with the nearest-neighbor distances in the crystalline phase. The small first peak in $g_{\text{Sn-Sn}}$ indicates the presence of a few Sn_2 dimers in the melt. This is also reflected in the instantaneous configuration shown in Fig. 7, where three Sn-Sn dumb-bells with a bond-length $\leqslant 3.6$ Å are displayed. On average, a Sn-atom in the melt has 0.24 Sn neighbors, compared to 0.5 in the crystalline structure. The calculation of the remaining coordination numbers is complicated due to the very different peak-shapes. For $N_{\text{Li-Sn}}$ integration over the symmetric part of the first peak leads to a value of 6.69, which is in very good agreement with the coordination in the crystalline phase ($N^{\text{cryst.}}_{\text{Li-Sn}} = 6$). For the Li-Li correlations, integration over the symmetric part of the first peak underestimates the coordination number considerably. Integration over the full peak up to the minimum at $R = 3.99$ Å yields $N_{\text{Li-Li}} = 9.59$, again in very good agreement with the average coordination number calculated for the crystal. The different way of calculating the partial coordination numbers is justified by the rather asymmetric distribution of the Li-Li distances in the crystalline phase.

2. Partial structure factors and neutron diffraction intensity

Figure 8 shows both the component-related partial static structure factors $S_{ij}(q)$, i,j=Li,Sn (we use the Ashcroft-Langreth definition of partial structure factors, unless otherwise stated), and the Bhatia-Thornton density-concentration structure factors $S_{NN}(q)$, $S_{Nc}(q)$, and $S_{cc}(q)$. The Sn-Sn structure factor shows a dominant ''prepeak'' at $q_p \sim 1.55$ Å, a much weaker ''structural'' peak at $q_1 \sim 2.6$ Å, and almost no higher order oscillations. The ratio of the positions of pre- and structural peak is with $q_p/q_1 \sim 0.6$ which is much larger than in the alloys of the heavier alkali metals with Sn, where we had found values ranging between 0.42 and 0.46. This indicates a rather different character of the short-range order. In the present case, this ordering is salt-like as a consequence

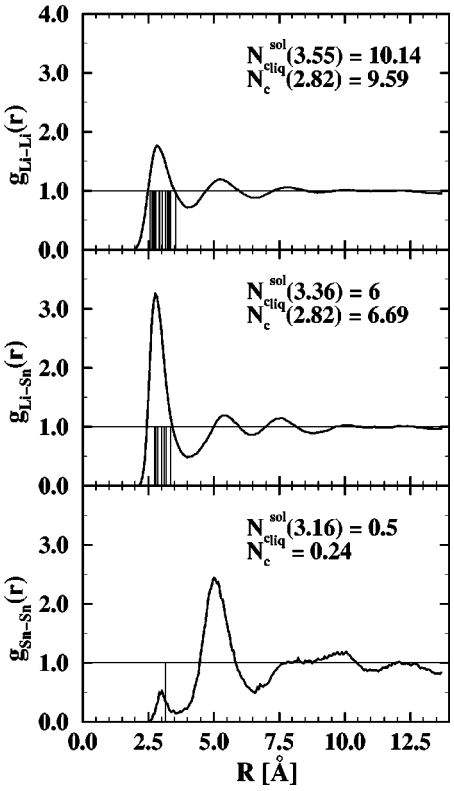

FIG. 6. Partial pair correlation functions $g_{ij}(R)$ $(i,j = \text{Li,Sn})$ for molten Li_4Sn at $T = 1040$ K. The vertical bars show the nearest-neighbor distances as calculated for the crystalline Li_7Sn_2 compound. The inset lists the partial coordination numbers calculated for the crystalline and liquid alloys, cf. text.

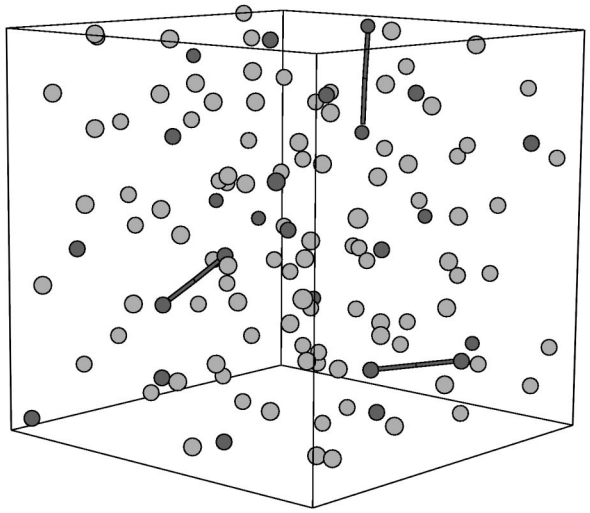

FIG. 7. Characteristic instantaneous configuration of molten Li_4Sn. Light balls: Li atoms, darks spheres: Sn atoms. The solid bars mark the nearest-neighbor bonds in the few existing Sn_2 dimers, cf. text.

of strong Li-Sn interactions; the formation of direct covalent Sn-Sn bonds plays only a minor role. The Li-Li structure factor shows a shoulder at the position of the prepeak, suggesting that the local arrangement of the Li atoms is also influenced by the strong chemical interactions. However, the analysis of the Bhatia-Thornton structure factors demonstrates that this does not lead to any substantial topological short-range order, as evidenced by the hard-sphere-like form of the density-fluctuation structure factor S_{NN}. The concentration fluctuation structure factor S_{cc}, on the other hand, shows only a single peak at the position of the prepeak in $S_{\text{Sn-Sn}}$ and almost no higher order oscillations. S_{Nc} is small everywhere as a consequence of the almost equal effective diameter of the Li and Sn atoms (see the peak positions in the correlation functions).

The neutron scattering amplitude for the natural isotope mixture of Li is negative due to the dominant contribution from the Li^7 isotope ($b_{\text{Li}}=-0.2147$, $b_{\text{Li}^7}=-0.234$, $b_{\text{Li}^6}=0.18$, $b_{Sn}=0.61$, according to Ref. 52); therefore, the contribution of the three Bhatia-Thornton partial structure factors varies strongly with composition. At a concentration of $c_{\text{Sn}}=26.4$ at.pct., the average neutron scattering amplitude is zero for natural Li; therefore, only the concentration fluctuations contribute to the observed diffraction intensity. For a pure Li^7 isotope, the zero alloy is at a concentration of $c_{Sn}=28.1$ at.pct. At the composition of the octet-alloy ($c_{Sn}=20$ at.pct.), the weighting factors of the three partials are $w_{cc}=5.97(5.79)$, $w_{Nc}=0.73(0.76)$, and $w_{NN}=0.022(0.30)$ (numbers in parentheses refer to an alloy prepared with isotopically pure Li^7); therefore, the neutron scattering intensity is strongly dominated by $S_{cc}(q)$. Our result reported in Fig. 9 is in very good agreement with the experimental results of Alblas *et al.*[29] on an isotopically enriched specimen. Unfortunately, the experimental results are limited to $q\leqslant 4$ Å^{-1} due to the use of a stainless steel crucible; therefore, the radial distribution functions calculated from the measured data are subject to a certain termination error. Nevertheless, the radial correlation function derived by Alblas *et al.* (which is dominated by the effect of the concentration fluctuations) is in good agreement with our calculations; see Fig. 10. This confirms that even medium-range chemical order is well described by the simulations.

B. Equiatomic alloys

For the equiatomic alloy at $T=764$ K we calculate an equilibrium atomic volume of $\Omega=22.1$ Å^3, which agrees

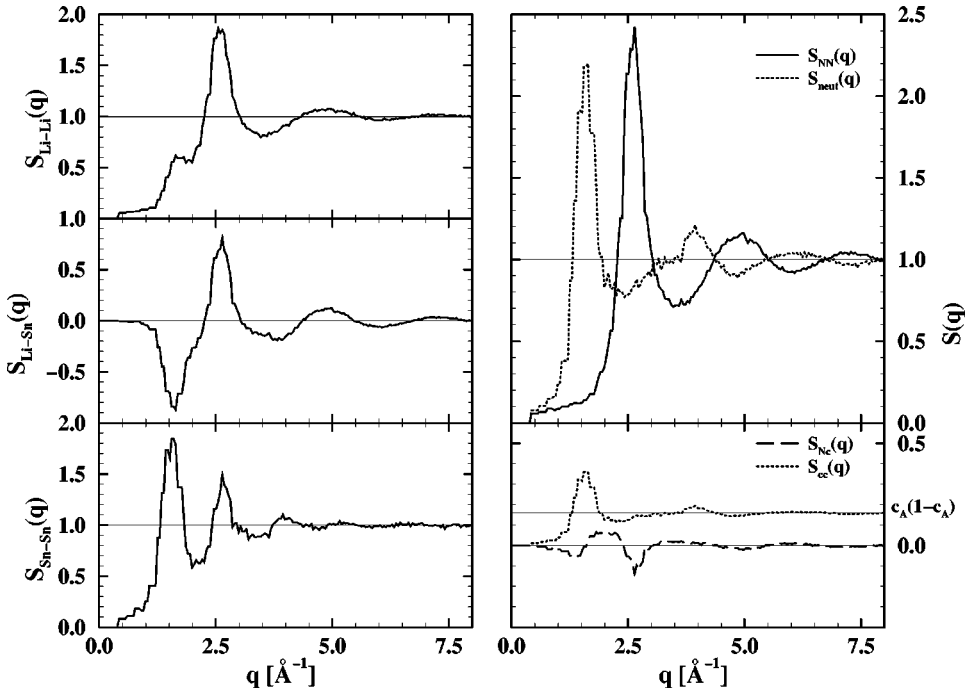

FIG. 8. Partial static structure factors $S_{ij}(q)$ for molten Li_4Sn at $T=1040$ K. Both the component-related ($i,j=$Li-Sn) and the Bhatia-Thornton density (N)-concentration (c) structure factors ($i,j=N,c$) are shown. The broken line in the right column shows the neutron-weighted total structure factor.

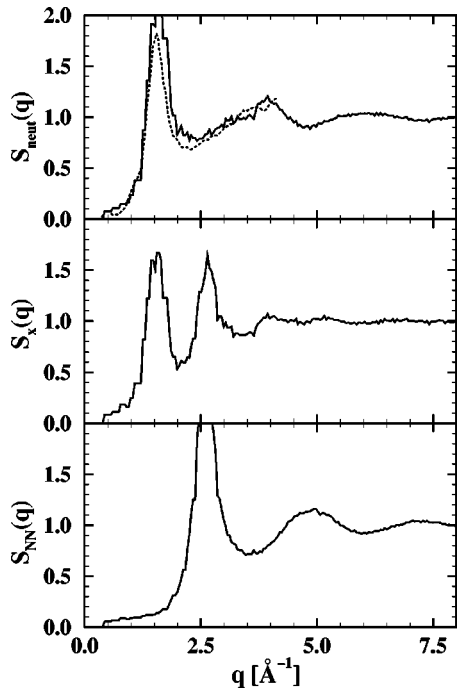

FIG. 9. Total neutron- and x-ray weighted static structure factors $S_{\mathrm{neut}}(q)$ and $S_X(q)$ for molten Li_4Sn at $T=1040$ K. For the neutron-weighted structure factor the experimental result of Alblas *et al.* (Ref. 29) is shown for comparison (dashed line).

reasonably well with the value $\Omega=23.2$ Å^3, deduced from the experimental volumes of the pure metals and assuming an excess volume of $\Delta\Omega\sim 15.3$ pct. equal to that in the crystalline phase (using again β-tin as reference). The pair correlation functions have already been presented in conjunction with our work on the alloys of Sn with the heavier alkali metals. The Li-Sn correlation function is almost identical to that calculated for Li_4Sn. We also observe only very small changes in the Li-Li correlations, mostly a weak damping of the higher order-oscillations. The Sn-Sn correlation function on the other hand is profoundly modified: a sharp nearest-neighbor peak at $R=2.98$ Å is indicative of the formation of strong Sn-Sn bonds leading to the formation of an entangled network of the Sn-atoms.[5] Compared to the crystalline LiSn-compound, the partial coordination number for heterocoordination $[N_{\mathrm{Li\text{-}Sn}}=7.45$ (liq.) and 8 (cryst.)] is almost unchanged. The Sn-Sn coordination number, on the other hand, is reduced from 4 in the crystal to 2 in the melt. This indicates again a change to a more salt-like structure on melting. Here we analyze only rather briefly the Bhatia-Thornton structure factors and the neutron- and x-ray diffraction intensities (see Fig. 11). The concentration fluctuation structure factor indicates a persistent chemical short-range ordering. For neutron-diffraction the contribution from the concentration fluctuations is still dominant (we calculate $w_{NN}=0.16$, $w_{cc}=3.34$, and $w_{Nc}=1.49$ using the scattering amplitudes of the Li^7 isotope), whereas for x-ray scattering there are also substantial contributions from the other partials ($w_{NN}=0.56$, $w_{cc}=1.76$, and $w_{Nc}=1.98$ in the long-wavelength limit). The x-ray diffraction results for liquid Li-Sn date back to the old work of Goebbels and Ruppersberg,[28] where the scattering intensity is expressed in terms of a weighted average of the Faber-Ziman partial structure factors, with the incoherent Laue intensity subtracted. In this form theory and experiment are compared in Fig. 11. To permit a direct comparison of neutron- and x-ray structure factors, we also show the x-ray structure factor, according to the convention used for the neutron data. The comparison with the combined experimental neutron- and x-ray data demonstrates that both chemical and topological ordering is well described by our simulations. We should also point out that pair correlation functions and structure factors are very similar to those calculated for liquid NaSn, but differ considerably from those of KSn. This supports our argument that in NaSn the polyanionic order present in the crystalline phase disappears on melting.

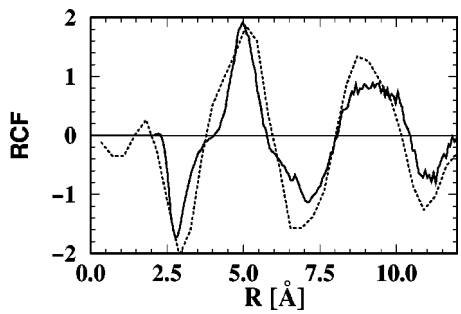

FIG. 10. Radial concentration correlation function $4\pi R^2 g_{cc}(R)$ for liquid Li_4Sn_2, compared with the experimental result of Alblas *et al.* (Ref. 29) (dashed line).

V. DYNAMICAL PROPERTIES

The dynamical properties of molten Li-Sn alloys are of particular interest because of the strong chemical short-range order, combined with a large mass ratio (the Sn atoms are about 17 times heavier than the Li atoms). In a binary liquid, concentration fluctuations coexist with density fluctuations. In the long-wavelength limit, the dynamical structure factor for density fluctuations is related to the isothermal compressibility, and the dynamical concentration fluctuations are inversely proportional to the thermodynamic excess stability (the second derivative of the free enthalpy with respect to concentration).[53] For a charged liquid this derivative becomes infinite to ensure charge neutrality, and infinite-wavelength concentration fluctuations are suppressed. The consequence for the dynamical properties is the existence of an optical mode or plasma oscillation with a finite frequency at $q=0$. In uncharged binary mixtures the excess stability is finite and hence there is no optical mode in the long-wavelength limit. Usually, it is also not possible to observe propagating concentration fluctuations because they contribute to the zero-frequency diffusive peak rather than to inelastic excitations (see, e.g., Jacucci and MacDonald[54]). The case of alloys with at least partial charge-transfer is hence of particular interest. The case of molten Li_4Pb alloys has been studied by both inelastic neutron scattering[55] and molecular dynamics simulations[56] based on the assumption of a screened Coulomb interaction between Li and Pb ions. The

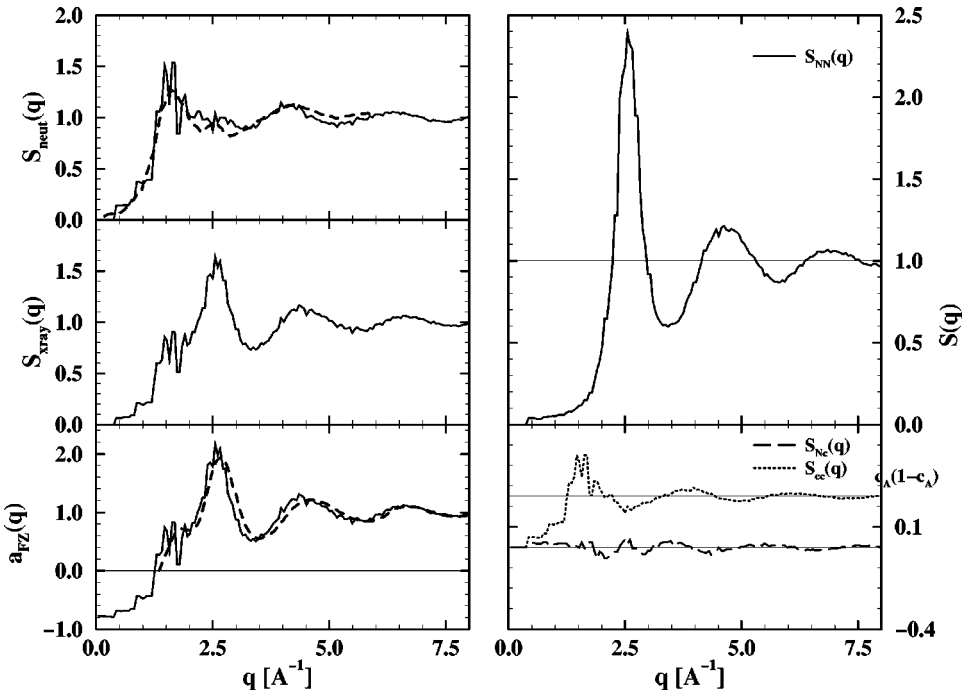

FIG. 11. Partial Bhatia-Thornton density (N)-concentration (c) structure factors $S_{ij}(q)(i,j=N,c)$ for LiSn at $T=765$ K (a) and neutron-weighted resp. x-ray weighted total structure factors $S(q)$, compared with the experimental results of Alblas *et al.* and Goebbels and Ruppersberg (Refs. 29 and 28). The experimental x-ray result is given in terms of a weighted average over the partial Faber-Ziman structure factors with the incoherent Laue scattering subtracted $[a_{\mathrm{FZ}}(q)]$. To facilitate comparison with the neutron result, we present also the x-ray structure factor calculated according to the convention adopted elsewhere in this paper.

fact that Li_4Pb has nearly zero average scattering amplitude for neutrons made it possible to observe propagating concentration fluctuations sustained by the light Li atoms. The existence of propagating concentration fluctuations at high frequency could be confirmed by the molecular dynamics simulations that also predicted the existence of a low-lying, almost dispersion-less density fluctuation mode supported by the heavier Pb atoms. However, the region of momentum transfers, where a hybridization of density and concentration modes is expected, was inaccessible to both neutron and computer experiments.

From our *ab-initio* simulations we can derive the time-dependent velocity autocorrelation function (VACF) $Z(t)=\langle\langle \vec{v}_l(t)\vec{v}_m(t)\rangle\rangle$ (the double brackets indicate averaging over atomic sites and different initial states) and its Fourier transform, the frequency distribution $\Psi(\omega)$. Because of the still rather limited time-span of the simulations, a Welch-window function has to be used to minimize truncation errors in the Fourier transform. Our results for both concentrations are shown in Figs. 12 and 13. The behavior of the Li atoms is found to be rather similar in both alloys: The VACF decays rather rapidly, forming a deep minimum after about 0.06 ps, where all higher order oscillations are strongly over-damped. This form of the VACF is characteristic for a strong ''cage-effect:'' a particle displaced from its equilibrium position is driven back to its original location due to collisions with the surrounding atoms. Because these collisions occur with particles of very different masses, a possible oscillatory motion is strongly over-damped. In the frequency distribution function $\Psi(\omega)$ this is reflected in a very large width of the inelastic peak centered around about 48 ps^{-1}, in good accordance with a period of $t\sim 0.13$ ps estimated from the first oscillation in the VACF. Slightly higher frequencies for inelastic excitations have been calculated for pure liquid Li at $T=470$ K.[43]

The single-particle dynamics of the Sn-atoms, on the other hand, is found to be strongly concentration dependent. In Li_4Sn the slow initial decay of the VACF is followed by long-time oscillations, and in the frequency spectrum this corresponds to a sharp inelastic peak at $\omega=10$ ps^{-1}. This corresponds rather well to the expected dispersion-less density fluctuation mode. The existence of a dominant inelastic mode is caused by the oscillations of the heavy Sn atoms in the cage of surrounding Li atoms—because of the light mass

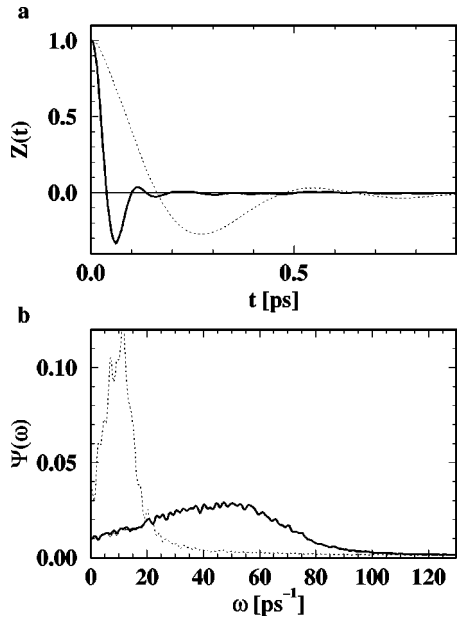

FIG. 12. Time-dependent velocity autocorrelation functions (VACF) $Z(t)$ of the ions in molten Li_4Sn and frequency distribution function $\Psi(\omega)$. Bold line: total; dashed line: Li; dotted line: Sn. The results referring to the total VACF and frequency distribution are almost indistinguishable from the Li-partials.

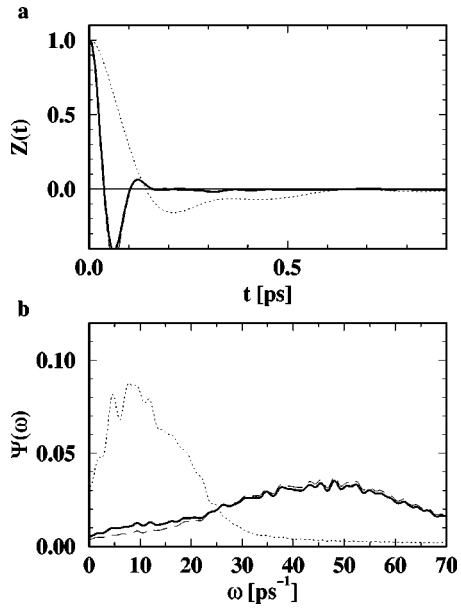

FIG. 13. Time-dependent velocity autocorrelation functions (VACF) $Z(t)$ of the ions in molten LiSn and frequency distribution function $\Psi(\omega)$. Bold line: total; dashed line: Li; dotted line: Sn.

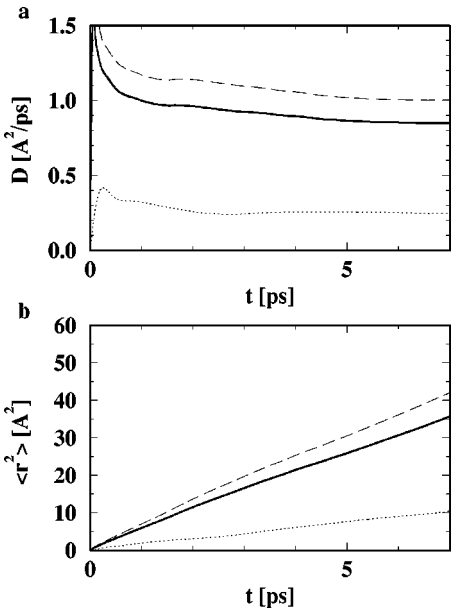

FIG. 14. Time-dependent mean-square displacement $\langle r^2(t)\rangle$ of the ions in molten Li_4Sn and diffusion constant D. Bold line: total; dashed line: Li; dotted line: Sn, cf. text.

of Li and the weak bonding between the atoms forming the cage, these collisions lead only to a rather weak damping.

In the equiatomic alloy, the VACF of the Sn atoms shows a rather complex behavior: the long-period oscillations are superposed by faster oscillations associated with vibrational movements in the strongly interconnected network of Sn-atoms. The partial frequency spectrum of the Sn atoms shows a rather broad distribution of inelastic excitations. It is rather similar to that calculated for liquid NaSn,[5] with a main peak at $\omega\sim 9$ ps and a shoulder at $\omega\sim 20$ ps^{-1}. In view of the similarity of the atomic structures, this is not at all unexpected.

We have not attempted to calculate partial dynamical structure factors for the molten alloys, although the results for pure liquid Li where certainly very encouraging.[43] The reason is that due to the small number of the minority atoms, the statistics for the dynamical structure factor of Sn will have a rather low accuracy. In addition, even for the present system size (which is very large for ab-initio MD simulations), the smallest accessible wave number is still $q_{\min}=0.46$ Å^{-1}, i.e., the region where the dispersion relations of the concentration- and density-fluctuation modes are expected to cross are still not accessible—this would require at least twice the number of atoms.

Diffusion constants may be derived from the low-frequency limit of the frequency distribution functions or from the long-time behavior of the mean-square displacements.[53] Figure 14 shows the mean-square displacements of Li and Sn atoms in molten Li_4Sn, together with the time-evolution of the diffusion constants. This figure illustrates the problems that have hampered earlier attempts to derive diffusion constants from very short *ab-initio* simulations: the diffusion constant converges only after about 6–7 ps, i.e., accounting for the need to average over different initial states, MD runs of at least 10 to 12 ps are required. Numerical values of the diffusion constants calculated for both alloys, together with reference values for the pure liquid metals, are compiled in Tables III and IV. For the alloys, the agreement between the diffusion coefficient calculated using both methods is not quite as good as for the pure metals. Discrepancies are most pronounced for the fast diffusing Li atoms, whereas we find good agreement for the more slowly diffusing Sn atoms.

The congruently melting near-octet compound has a high melting temperature. At these high temperatures, both atomic species diffuse faster in the alloy than in the pure molten metals at their respective low melting points. However, this enhancement is only modest for Sn; and it is also important to emphasize that the ratio D(Li)/D(Sn) ~ 4 is larger than the ratio of the diffusion coefficients of the pure metals. This reflects the strong interaction between Sn and Li which tends to confine the Sn atoms to their ''cage'' formed by the much more mobile Li atoms.

For the equiatomic alloy, the strong chemical interactions

TABLE III. Parameters for *ab-initio* molecular dynamics simulations of molten lithium-tin alloys.

	Li_4Sn	LiSn
Number of atoms	125	124
Mass of alkali atom (a.u.)	6.94	6.94
Mass of Sn atom (a.u.)	118.71	118.71
Atomic volume (Å^3)	20.68	22.13
Number density (Å^{-3})	0.048	0.045
Temperature (K)	1040	765
Nosé mass (a.u.)	2.0	2.0
Time-steps (fs)	3	3
Duration of simulation (ps)	10.5	12.3

TABLE IV. Total and atom-specific diffusion constants in molten Li-Sn alloys and in pure liquid Li and Sn, calculated from the time-dependence of the mean-square displacement (MSD) functions and from the low-frequency limit of the frequency distribution functions are given. For comparison we note the diffusion constants of the pure metals at their respective melting points.

System	T [K]	D_{tot}		D_{Li} [$Å^2 ps^{-1}$]		D_{Sn}		
		VACF	MSD	VACF	MSD	VACF	MSD	exp.
Li	470			0.75	0.69			0.65 [a]
Li_4Sn	1040	1.02	0.85	1.21	1.00	0.27	0.25	
LiSn	765	0.27	0.20	0.37	0.24	0.17	0.17	
Sn	520					0.22	0.18	0.20 [b]

[a]After Ref. 57.
[b]After Ref. 58.

lead to a considerable slowing-down of the diffusive motion of both species. This is particularly pronounced for the Li atoms, whose diffusive motion is hindered by their strong interaction with the dense network formed by the Sn ions. It is also interesting to compare the diffusion constants for liquid LiSn with those of the corresponding alloys of the heavier alkali metals, where polyanions are formed (at least in the crystalline phase). In liquid NaSn, where the polyanions are almost completely destroyed on melting, we find $D(\mathrm{Na}) = 0.26\ Å^2\ ps^{-1}$ and $D(\mathrm{Sn}) = 0.19\ Å^2\ ps^{-1}$, i.e., values that are very similar to those we find here for LiSn: $D(\mathrm{Li}) = 0.30\ Å^2\ ps^{-1}$, $D(\mathrm{Sn}) = 0.17\ Å^2\ ps^{-1}$ (we take the average over the VACF and MSD results). This, together with the similarity of the atomic structure we have already noted, suggests that the atomic order is very similar in liquid LiSn and NaSn. In liquid KSn, where a substantial fraction of the Sn_4 polyanions subsist in the liquid phase, diffusion is much faster for the larger K atoms. This can only be understood when we consider that, due to the formation of saturated covalent bonds within the polyanions, the interaction between K and Sn atoms are much weaker than in the alloys of Sn with the lighter alkalis.

VI. ELECTRONIC STRUCTURE

Finally, we turn to the analysis of the electronic structure of the molten Li-Sn alloys. The electronic density of states (DOS) has been calculated for a number of representative configurations, using for each model a grid of Monkhorst-Pack special points in the small Brillouin-zone corresponding to the MD cell. This is important in order to avoid the appearance of unphysical structures in the DOS. Our results for

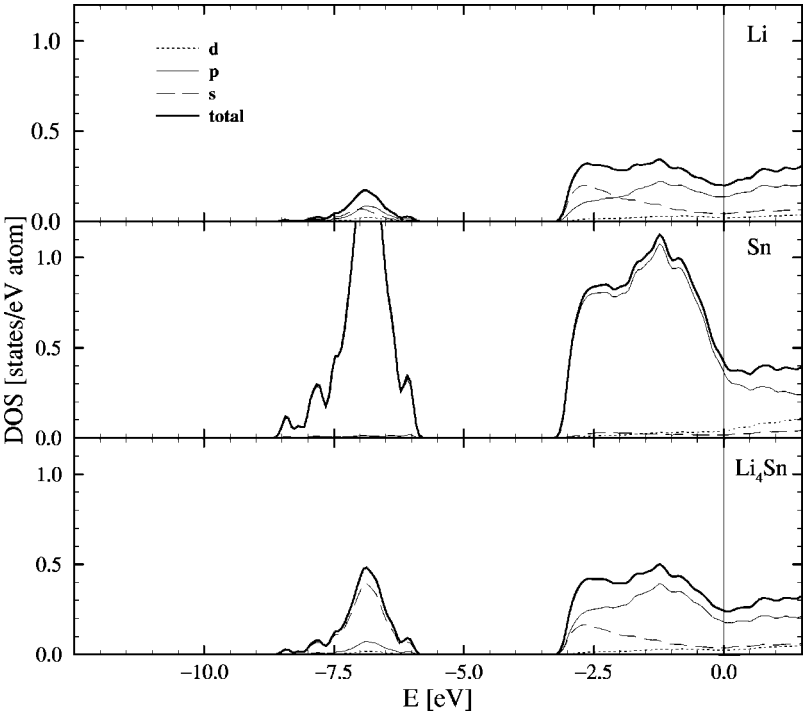

FIG. 15. Total and partial electronic densities of state of liquid Li_4Sn.

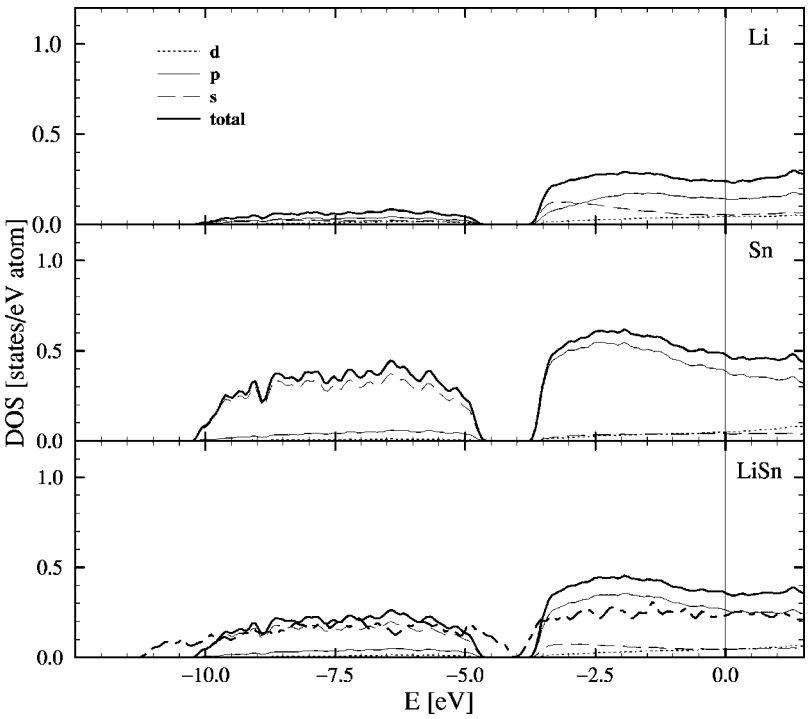

FIG. 16. Total and partial electronic densities of state of liquid LiSn. The dot-dashed line shows for comparison the electronic density of states in pure molten tin.

both compositions are displayed in Figs. 15 and 16. The DOS of the molten octet alloy is strongly dominated by Sn-states, in analogy to the crystalline compound: the atomic spheres surrounding the Li-sites are not completely depleted of electrons as expected from a naive charge-transfer picture, but the partial DOS calculated for the atomic spheres surrounding the Li-site has a strongly mixed angular-momentum character for occupied states, suggesting that this DOS arises in reality from extended Sn-p states overlapping into the Li-spheres. This is completely analogous to the situation in other Zintl alloys. The Fermi level falls into a shallow minimum of the DOS—this explains the resistivity maximum found at this composition. Above the Fermi-level, the contribution of the Sn-states to the total DOS is strongly reduced. The DOS of liquid Li_4Sn differs from that of the crystalline compound Li_7Sn_2 (see Fig. 4) in several characteristic features. (i) The Sn-*p* band just below the Fermi level is narrower than in the crystalline phase. Part of this change has certainly to be attributed to a reduced band-filling due to a slightly reduced Sn-content in the molten alloy. However, one would expect that this reduction is over-compensated by a smearing of the band induced by the thermal disorder. (ii) Instead of the split Sn-*s* band at higher energies (the splitting arises from the formation of $ss\sigma$ bonds in the Sn_2 dimers), we find a unimodular DOS with only a weak tail at the position of the lower part of the split band. Both the reduction of the *p*-band width and the absence of *s*-band splitting reflect the reduced role of direct Sn-Sn interactions in the molten alloy, in accordance with our analysis of the atomic structure.

The DOS of the molten equiatomic alloy shows a roughly semi-elliptic Sn-*s* band extending from -10.2 eV to about -4.6 eV and an almost rectangular Sn-*p* band between -3.6 eV and the Fermi level, i.e., we find an internal gap of about 1 eV which is absent in the corresponding crystalline phase. Otherwise, the spectra of the crystalline and molten alloys are very similar. The formation of such an internal gap separating *s*- and *p*-bands reflects the reduction of *s*-*p* hybridization due to thermal disorder. The DOS of liquid LiSn is also very similar to that of molten Sn.[59,44] The only difference is that due to the higher Sn-Sn coordination number, both sub-bands are broadened so that the internal gap shrinks almost to zero. Again, this shows that the strong *s*,*p* hybridization characteristic for α-Sn (and, although to a reduced degree, also for β-tin) breaks down due to thermal disorder. The existence of of such a deep DOS-minimum in liquid Sn is well confirmed by photoelectron spectroscopy.[60] An extension of these studies to molten Zintl-alloys would evidently be of the greatest interest.

VII. DISCUSSION AND CONCLUSIONS

We have presented detailed local-density-functional investigations of crystalline and molten Li-Sn alloys at the ''octet'' and equiatomic compositions, with the aim of elucidating eventual covalent contributions to the chemical bonding in these materials. For crystalline LiSn we find that the LDF calculations predict the unique structure of this alloy, where the Sn-atoms form rumpled atomic layers similar to those existing in crystalline As, to be lower in energy than the simple ionic CsCl lattice realized in the homologous compound LiPb. Evidently, this is due to the stronger tendency of the Sn atoms to form homoatomic covalent bonds, the layered arrangement of the Sn-ions corresponds to the crystal structure of the isoelectronic element As, in accordance with the generalized Zintl principle. Upon compression, a phase transition to the more metallic CsCl structure is predicted. For crystalline Li_7Sn_2 (which is the composition closest to the octet stoichiometry Li_4Sn realized in this system) we find that the structurally related Li_7Sn_2 and Li_7Pb_2

lattices are energetically almost degenerate (the structural energy difference is $\Delta E \leqslant 5$ meV/atom at equilibrium). In the Li_7Sn_2 structure half of the Sn atoms form Sn_2 dimers (here the structural and electronic analogy is with the diatomic molecules in halogen crystals), whereas in Li_7Pb_2 structure the nearest-neighbor Pb-Pb distance is maximized. In this case, the energy gain realized by forming covalent Sn-Sn bonds in the dimers is, in our calculation, just not sufficient to overcompensate the deficit in the electrostatic energy. At the present moment, the reason for the failure of the LDF calculations to predict the correct crystal structure remains unclear. Gradient corrections to the exchange-correlation functional are unlikely to change the picture. In a large number of calculations it has been found that at a given volume, LDA and GGA lead to identical structural predictions. The gradient corrections merely increase the equilibrium volume. If the GGA would change the structure at all, an elongation of the Sn-Sn bonds could only make agreement with experiment worse. Altogether, a convenient choice of a DFT functionals seems to be particularly difficult for compounds with such large differences in valence and atomic number.

Extended *ab-initio* MD simulations have been performed for the liquid alloys. At the octet composition our calculated structure agrees very well with the neutron diffraction data of Alblas *et al.*[29] (which, however, test mainly the concentration fluctuations). At the equiatomic composition we find good agreement with both the neutron- and x-ray-scattering results[29,28] reported in the literature, thus confirming in detail the predictions concerning chemical—as well as topological short- and medium-range ordering. In Li_4Sn we find only a very small number of Sn_2 dimers; the dominant feature of the chemical short-range order is heterocoordination. Thus the liquid structure is salt-like (in analogy to molten Li_4Pb), with only weak covalent bonding effects. In molten LiSn, on the other hand, we find also strong covalent Sn-Sn bonds, in analogy to our previous results for molten NaSn. The MD-simulations have been extended over time-intervals sufficient to allow a detailed analysis of the single-particle dynamics in the molten alloys. A strong composition dependence of the Sn-dynamics is detected. At the octet composition (where almost all Sn-atoms are surrounded by Li atoms only), the VACF of the Sn atoms shows long-time oscillations, leading to a sharp inelastic peak in the frequency distribution function. This behavior is due to a strong cage-effect, i.e. oscillatory movements of the heavy Sn-atoms in the cage of the light surrounding Li atoms. At the equiatomic composition, the Sn-dynamics is more complex due to the strong bonding in the disordered network of Sn-Sn bonds. We have also calculated interdiffusion constants, finding that the chemical ordering enhances the difference in the diffusion constants, with the diffusion of the Sn atoms being slowed down by the strong bonds in the covalently bonded Sn-network and/or to the surrounding Li-cage.

The calculated electronic spectra of both crystalline and molten alloys demonstrate that the valence electron-spectrum is dominated by the strong attractive potential of the Sn atoms. In analogy with our analysis of the alloys of Sn with the heavier alkali metals, we find that spatial charge transfer is small (the atomic spheres surrounding the Li atoms remain essentially charge-neutral), but the Zintl picture is nevertheless appropriate because the character of the eigenstates is distinctly Sn-like. In this sense, it is legitimate to speak of charge-transfer alloys. The difference between, e.g., K-Sn and Li-Sn is in the different size of the alkali ion: at the equiatomic composition the smaller Li atoms cannot separate eventual Sn_4 polyanions to the extent to prevent the formation of inter-cluster bonds destabilizing the polyanions. On the other hand, at the octet composition, the Li ions are sufficiently small to allow the formation of a screening cage of Li ions surrounding the Sn anions, thus reducing electrostatic repulsions.

In summary, the present work extends our previous studies of Zintl-alloy formation,[5,24,25] confirming the validity of a generalized Zintl principle: In the K-Sn and Na-Sn systems[5], electron transfer leads to an s^2p^3 valence-electron configuration of the Sn ions and to polyanion-formation promoted by strong covalent bonds, in analogy to the formation of P_4 molecules in phosphorus vapor. The large separation between the polyanions caused by the large diameter of the *K* ions is analogous to the dilution in the vapor phase, and is sufficient to stabilize the polyanions even in the liquid phase. In Na-Sn and in LiSn this is not the case. Instead of isolated compact polyanions, extended Sn networks (corrugated layers in the crystalline, three-dimensional networks in the molten phase) are formed, in analogy with the denser crystalline forms of the pnictide elements (As, Sb). In NaSn this happens in the the liquid phase only, polyanions are stable in the crystalline state. In LiSn polyanions are unstable in both the liquid and solid phases. In the K-Sb system we had already analyzed a situation where a gradual transition from polyanionic to simple ionic (salt-like) bonding occurs with increasing K-content: at the equiatomic composition, electron transfer leads to a valence-electron configuration isoelectronic to Se, promoting the formation of Se-like polyanionic chains. Increasing K allows to saturate dangling bonds at the chain-ends, leading to a progressive shortening of the . . . -Sb-Sb- . . . chains, culminating in a salt-like structure with no polyanions in K_3Sb.[25] The Li-Sn system shows a similar trend. In the equiatomic alloy, electron transfer leads to the same s^2p^3 configuration as in KSn, but as the polyanions cannot be kept at sufficiently large distances from each other, an As-like arrangement of the Sn atoms on rumpled planes is stabilized in the crystalline phase. In the melt a dense disordered Sn-network is formed. At larger Li-content, the trend is again towards a simple ionic structure, but in the crystalline phase (and to a lesser degree in the melt) covalent interactions stabilize a certain extent of Sn-pairing. However, we have to emphasize that this effect appears to be underestimated by the LDA calculations. Polyanionic dimers are found in alkali-chalcogenide alloys.[61] Their presence in the Li_4Sn octet alloys would suggest that, in this case, charge transfer is not complete, so that saturation of the chemical bonds can be achieved only through polyanion formation. In this context, it is also worthwhile to mention the work on Li-Si[27] and Li-Ga alloys[24] (although the latter study has not been performed *ab-initio*, but is based on effective pair interactions). In this system, increasing Li content leads to an increasing occupation of the Ga-*p* states with the Ga ions

becoming progressively isoelectronic to Ge, As, and Se. This is reflected by the formation of crystalline compounds with the Ga-ions forming a diamond-type sublattice, rumpled layers, and isolated chains and disordered Ga-networks with decreasing coordination numbers in the melt, together with the corresponding signature in the electronic spectra. In the *ab-initio* MD-simulations of Li-Si alloys with about 65 at-.pct. Li, an analogy between the star- and ring-like polyanions in the crystalline compounds and the dense Si-network in the melt, with the structure of S- or Se-clusters and the structures of the molten chalcogenides has been drawn. Altogether, a sound quantum-mechanical foundation for the old Zintl concepts begins to emerge.

Note added in proof. Very recently, the stability of different four-connected networks of the polyvalent atoms in alloys of Li with Sn, Sb, and Te has been discussed by Ienco *et al.*[62] on the basis of extended Hückel theory. It was pointed out that the large differences in the bond strength of the isoelectronic compounds of these elements arise from different degrees of admixture of antibonding states to the highest occupied band, the antibonding character being stronger for Sn than for Sb or Te in accordance with the more extended nature of the Sn orbitals. We thank Professor Hoffmann for bringing this work to our attention.

ACKNOWLEDGMENTS

This work has been supported by the Austrian Science Funds under Project Nos. P10445-PHYS and P11353-PHYS and by the Austrian Ministry for Science through the Center for Computational Materials Science.

[1] E. Zintl and G. Brauer, Z. Phys. Chem. Abt. B **20**, 245 (1933).
[2] E. Zintl and G. Wolterdorf, Z. Elektrochem. **41**, 876 (1935).
[3] F. Springelkamp, R. A. de Groot, W. Geertsma, W. van der Lugt, and F. M. Mueller, Phys. Rev. B **32**, 2319 (1985).
[4] M. Tegze and J. Hafner, Phys. Rev. B **39**, 8263 (1989).
[5] O. Genser and J. Hafner, J. Phys.: Condens. Matter **13**, 959 (2001); **13**, 981 (2001).
[6] M. Tegze and J. Hafner, Phys. Rev. B **40**, 9841 (1989).
[7] W. Geertsma, J. Dijkstra, and W. van der Lugt, J. Phys. F: Met. Phys. **14**, 1833 (1984).
[8] W. van der Lugt and W. Geertsma, Can. J. Phys. **65**, 326 (1987).
[9] R. Winter, in *Thermodynamics of Alloy Formation*, edited by Y. A. Chang and F. Sommer (The Minerals, Metals and Materials Society, London, 1997), p. 143.
[10] M. L. Saboungi, J. Fortner, W. S. Howells, and D. L. Price, Nature (London) **365**, 237 (1993).
[11] G. Galli and M. Parrinello, J. Chem. Phys. **95**, 7504 (1991).
[12] G. Seifert, G. Pastore, and R. Car, J. Phys.: Condens. Matter **4**, L179 (1992).
[13] M. Schöne, R. Kaschner, and G. Seifert, J. Phys.: Condens. Matter **7**, L19 (1995).
[14] G. Seifert, R. Kaschner, M. Schöne, and G. Pastore, J. Phys.: Condens. Matter **10**, 1175 (1998).
[15] O. Genser and J. Hafner, J. Non-Cryst. Solids **250-252**, 236 (1999); J. Hafner, K. Seifert-Lorenz, and O. Genser, *ibid.* **250-252**, 225 (1999).
[16] J. F. Smith and Z. Moser, J. Nucl. Mater. **59**, 158 (1976).
[17] D. M. Bailey, W. H. Skelton, and J. F. Smith, J. Less-Common Met. **64**, 233 (1979).
[18] A. Zalkin and W. J. Ramsey, J. Phys. Chem. **60**, 234 (1956).
[19] U. Frank, W. Müller, and H. Schäfer, Z. Naturforsch. B **30**, 6 (1975).
[20] A. Zalkin and W. J. Ramsey, J. Phys. Chem. **62**, 689 (1958).
[21] W. Müller and H. Schäfer, Z. Naturforsch. B **28**, 246 (1973).
[22] E. Busmann, Z. Anorg. Allg. Chem. **313**, 90 (1961).
[23] J. Witte, H.G. von Schnering, and W. Klemm, Z. Anorg. Allg. Chem. **327**, 260 (1964).
[24] J. Hafner and W. Jank, Phys. Rev. B **44**, 11 662 (1991).
[25] K. Seifert-Lorenz and J. Hafner, Phys. Rev. B **59**, 829 (1999); 843 (1999).
[26] R. Nesper, H.G. von Schnering, and J. Curda, Chem. Ber. **119**, 3376 (1986).
[27] G. de Wijs, G. Pastore, A. Selloni, and W. van der Lugt, Phys. Rev. B **48**, 13459 (1993).
[28] K. Goebbels and H. Ruppersberg, in *The Properties of Liquid Metals*, edited by S. Takeuchi (Taylor and Francis, London, 1973), p.63.
[29] B. P. Alblas, W. van der Lugt, J. Dijkstra, W. Geertsma, and C. van Dijk, J. Phys. F: Met. Phys. **13**, 2465 (1983).
[30] M. S. Foster, C. E. Crouthamel, and S. E. Wood, J. Phys. Chem. **70**, 3042 (1966).
[31] A. K. Fischer and S. A. Johnson, J. Chem. Eng. Data **17**, 280 (1972).
[32] C. Van der Marel, A. B. van Oosten, W. Geertsmaa, and W. van der Lugt, J. Phys. F: Met. Phys. **12**, 2349 (1982).
[33] C. Van der Marel, W. Geertsmaa, and W. van der Lugt, J. Phys. F: Met. Phys. **10**, 2305 (1980).
[34] G. Kresse and J. Hafner, Phys. Rev. B **48**, 13 115 (1993); **49**, 14 251 (1994).
[35] G. Kresse and J. Furthmüller, Comput. Mater. Sci. **6**, 15 (1996); Phys. Rev. B **54**, 11 169 (1996).
[36] J. Hafner and G. Kresse, in *Properties of Complex Inorganic Compounds*, edited by A. Gonis, A. Meike, and P. E. A. Turchi (Plenum, New York, 1997), p. 69.
[37] J. Perdew and A. Zunger, Phys. Rev. B **23**, 5048 (1981).
[38] D. M. Wood and A. Zunger, J. Phys. A **18**, 1343 (1985).
[39] P. Pulay, Chem. Phys. Lett. **73**, 393 (1980).
[40] S. Nosé, J. Chem. Phys. **81**, 511 (1984).
[41] D. Vanderbilt, Phys. Rev. B **41**, 7892 (1990).
[42] G. Kresse and J. Hafner, J. Phys.: Condens. Matter **6**, 8245 (1994).
[43] G. Kresse, J. Non-Cryst. Solids **205-207**, 833 (1996).
[44] O. Genser and J. Hafner, Phys. Chem. Liq. (unpublished).
[45] H. J. Monkhorst and J. D. Pack, Phys. Rev. B **13**, 5188 (1976).
[46] P. Blöchl, O. Jepsen, and O. K. Andersen, Phys. Rev. B **49**, 16 223 (1994).

[47] D. C. Wallace, *Thermodynamics of Crystals* (Wiley, New York, 1972).
[48] G. Kresse, J. Furthmüller, and J. Hafner, Phys. Rev. B **50**, 13 181 (1994).
[49] K. Seifert, J. Hafner, J. Furthmüller, and G. Kresse, J. Phys.: Condens. Matter **7**, 3683 (1995).
[50] H. Ruppersberg and W. Speicher, Z. Naturforsch. A **31**, 47 (1976).
[51] Y. Waseda, *The Structure of Non-Crystalline Materials* (McGraw-Hill, New York, 1980).
[52] G. E. Bacon, Acta Crystallogr., Sect. A: Cryst. Phys., Diffr., Theor. Gen. Crystallogr. **28**, 357 (1972).
[53] J.P. Hansen and I.R. MacDonald, *Theory of Simple Liquids* (Academic Press, London, 1976).
[54] G. Jacucci and I. R. McDonald, in *Liquid and Amorphous Metals*, edited by E. Lüscher and H. Coufal (Sijthoff and Noordhoff, Alphen van den Rijn, 1980).
[55] M. Soltwisch, D. Quittmann, H. Ruppersberg, and J. B. Suck, Phys. Rev. B **28**, 5583 (1983).
[56] M. Ronchetti, and G. Jacucci, in *Amorphous and Liquid Materials*, edited by E. Lüscher, G. Fritsch, and G. Jacucci (Martinus Nijhoff, Dordrecht, 1987).
[57] J.S. Murday and R.M. Cotts, Z. Naturforsch. A **26**, 85 (1971).
[58] T. Iida and R. I. L. Guthrie, *The Physical Properties of Liquid Metals* (Oxford Science, Oxford, 1988).
[59] W. Jank and J. Hafner, Phys. Rev. B **41**, 1497 (1990).
[60] G. Indlekofer, P. Oelhafen, R. Lapka, and H.J. Güntherodt, Z. Phys. Chem., Neue Folge **157**, 465 (1988).
[61] P. Böttcher, Angew. Chem. **27**, 759 (1988).
[62] A. Ienco, R. Hoffmann, and G. Papoian (unpublished); see also G. Papoian and R. Hoffmann, Angew. Chem. Int. Ed. Engl. **39**, 2408 (2000).